

FULL PAPER

Open Access



Recurrent partial resetting of quartz OSL signal by earthquakes: a thermochronological study on fault gouges from the Atotsugawa Fault, Japan

Sumiko Tsukamoto^{1,2*} , Benny Guralnik³, Erick Prince⁴, Kiyokazu Oohashi^{5,6} and Makoto Otsubo⁶

Abstract

Optically stimulated luminescence (OSL) dating utilises the detection of trapped charge in minerals, and has an ultralow closure temperature. There is the potential for direct dating of fault movement using fault gouges, because frictional heating caused by large earthquakes can reduce the OSL signal intensity of minerals within gouges. In this study, we conducted quartz OSL dating on four fault gouge and breccia samples from a surface outcrop of the Atotsugawa Fault, one of the most active dextral strike-slip faults in central Japan, where the last large earthquake occurred in AD1858, with an estimated magnitude of 7. The natural OSL signal intensity of fine-grained quartz was clearly below the signal saturation level, with the fraction of saturation (n/N) between 0.30 ± 0.02 and 0.39 ± 0.03 , indicating there was signal resetting by past earthquakes. However, the apparent OSL ages ranged from 22 ± 1 to 72 ± 4 ka, two orders of magnitude older than the age of the last earthquake. To explain the significant age over-estimation, we measured the thermal stability of the OSL signal, and used a thermal model with punctuated episodic losses to constrain the average shear heating temperature experienced during an individual faulting event. For an independently known recurrence interval of 2.5 ka and a presumed shear heating duration of 1 s, the observed n/N and the measured thermal stability of the OSL signals correspond to a resetting temperature of ~ 300 °C during a single earthquake event.

Keywords Active faults, Fault gouge, Fault activity, Optically stimulated luminescence dating, Partial resetting, Atotsugawa Fault

*Correspondence:

Sumiko Tsukamoto

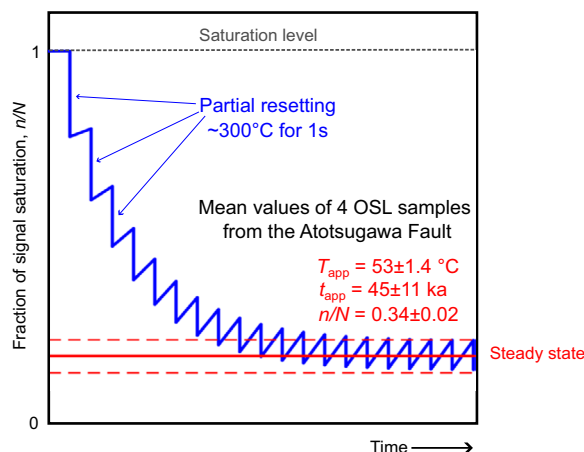
sumiko.tsukamoto@leibniz-liag.de

Full list of author information is available at the end of the article



© The Author(s) 2024. **Open Access** This article is licensed under a Creative Commons Attribution 4.0 International License, which permits use, sharing, adaptation, distribution and reproduction in any medium or format, as long as you give appropriate credit to the original author(s) and the source, provide a link to the Creative Commons licence, and indicate if changes were made. The images or other third party material in this article are included in the article's Creative Commons licence, unless indicated otherwise in a credit line to the material. If material is not included in the article's Creative Commons licence and your intended use is not permitted by statutory regulation or exceeds the permitted use, you will need to obtain permission directly from the copyright holder. To view a copy of this licence, visit <http://creativecommons.org/licenses/by/4.0/>.

Graphical Abstract



1 Introduction

Evaluation of the activity of faults is one of the most important requirements to prepare for future disastrous earthquakes. Previous attempts to evaluate recent fault activity were performed mainly where active faults cut Quaternary sediments and/or landforms and the timing of their past activities was then estimated by using fault-displaced sediments that contain datable materials. For instance, if a fault cuts a young fluvial or colluvial sediment, the ages of past movements can be estimated by radiocarbon dating of organic matters or luminescence dating the sediment (e.g. Okumura 2001; Fattahi and Walker 2007; Chen et al. 2009). For this approach, the dating methods are well established, although this is an indirect dating method for faulting, and the relationship between the age and the earthquake events is not always clear.

In Japan, the activities of many faults were studied extensively, and the data including the strike direction, slip, length, mean slip rate, as well as recurrence interval were documented (Research Group for Active Faults of Japan 1991). However, active faults do not always cut young, outcropping sediments, nor are they covered by young sediments that can be viably dated. This means that for many faults, which have been mapped geologically or geomorphologically, there has been until now no direct method available to evaluate their activity.

Direct dating of fault movement can be carried out with thermochronological investigation of fault rocks using dating methods, because the frictional heating caused by fault motion can partially or totally reset the “clock” of the dating methods (Tagami 2005, 2012; Tsukamoto et al. 2020). For instance, the Nojima Fault, which

was responsible for the Mw 6.9 Hyogo-ken Nanbu Earthquake (Kobe Earthquake) of 1995 in Japan, was investigated using zircon fission-track at different depths of core samples (Tagami and Murakami 2007). Direct dating of faults has been also conducted using K/Ar dating of authigenic clay minerals in fault gouges from the Nojima Fault (Zwingmann et al. 2010). However, due to the relatively high closure temperatures, these methods were not applicable to evaluate the most recent activity of the fault.

Luminescence and electron spin resonance (ESR) dating methods using quartz and feldspar have recently been developed as ultralow temperature thermochronometers and thermometers (e.g. Herman et al. 2010; Guralnik et al. 2013, 2015; King et al. 2016, 2020), building on earlier studies from the 1970’s that employed the thermoluminescence (TL) signal (Durrani et al. 1972, 1973, 1977). The earliest attempt to date fault gouges directly using ESR signals can be traced to Ikeya et al. (1982). These authors dated gouges and breccias from the fault core of the Atotsugawa Fault, central Japan, at various distances from the main fault plane, using the quartz E’ centre. The ages decreased towards the fault plane and the youngest age calculated was 65 ka, although the latest earthquake on this fault is known to be AD1858 (Hietsu Earthquake, estimated magnitude 7). After this pioneering study, the method was tested using multiple centres of quartz ESR including the E’, Al, Ge, and oxygen hole centres (e.g. Fukuchi 1989), as well as different grain sizes (e.g. Lee and Schwarcz 1994). The latter authors proposed the grain-size plateau method; they consider the ESR signals were fully reset by the last earthquake, if an age plateau towards the smaller grain sizes of quartz in the fault gouge exists.

Ganzawa et al. (2013) used quartz OSL and thermoluminescence (TL) signals to date a fault gouge sample from the Atotsugawa Fault. They obtained an age of 200 ± 200 a from the OSL of a sand-sized quartz sample, which is consistent with the AD1858 Hietsu Earthquake. However, the TL age calculated from the 270°C TL peak was ~ 190 ka for the same sample. From the San Andreas Fault Observatory at Depth, 2.6 km below the surface, Spencer et al. (2012) used K-feldspar grains from gouge samples and obtained an infrared stimulated luminescence age of 139 ± 12 a (before 2010), where the largest historical earthquake of Mw 7.9 Fort Tejon Earthquake was occurred in AD1857. More recently, Tsakalos et al. (2020) used silt-sized quartz samples from a deep drilling core of the Nojima Fault. They sliced the fault gouge at a depth of 506 m into ~ 20 subsamples along the layering structure of the gouge to find whether the OSL signal from any of the thin layers had been completely reset by the Kobe Earthquake. The quartz OSL ages, however, ranged from 62.8 ± 4.3 to 18.5 ± 1.3 ka, three orders of magnitude older than the known age of the most recent event. Prince et al. (2024) studied fault gouge samples taken at the surface outcrops of different parts of the Periadriatic Fault System, Eastern Alps. They obtained saturated feldspar OSL ages and non-saturated quartz ESR ages from the Al centre, and assumed the last activity of the fault occurred between the minimum OSL and maximum ESR ages.

Despite the ultralow closure temperature of the discussed trapped charge dating methods, it has been the rule rather than exception, that OSL and ESR ages of faults overestimate the dates of historical earthquakes, often by orders of magnitude. This shows an urgent need for further investigation, assuming that signal resetting during large earthquakes is likely only partial, especially when gouge samples originate from surface outcrops or shallow subsurfaces.

In this study, we report quartz OSL ages from four gouge and breccia samples from a surface outcrop of the Atotsugawa Fault, central Japan. By analysing the data within the framework of OSL thermochronometry, we show that the apparent overestimation of the ages can be explained by a repetitive partial resetting by heating during past earthquakes. We convert the fraction of signal saturation (n/N) to the apparent temperature (mean storage temperature), which should be a function of the activity on the fault. Further, we calculate average partial resetting conditions at past earthquakes, which led to the apparent ages.

2 OSL thermochronometry and thermometry

In this section, we briefly introduce the theory of OSL thermochronology and thermometry for the quartz OSL following Guralnik et al. (2013) and Guralnik and

Sohbati (2019). In conventional OSL dating, an OSL age (t_{app}) is expressed by:

$$t_{\text{app}} = \frac{D_e}{\dot{D}} \quad (1)$$

where D_e is the equivalent dose, and \dot{D} is the environmental dose rate (e.g. Aitken 1985). Under transient conditions of simultaneous charge accumulation and thermal loss with the first-order kinetics, the apparent age in Eq. (1) can be simulated via:

$$\frac{dn}{dt} = \frac{\dot{D}}{D_0}(N - n) - Kn \quad (2)$$

where n is the number of filled electron traps, $N = \text{const}$ the number of available traps, D_0 is the characteristic saturation dose, and K is a thermal loss coefficient, given by:

$$K(T) = se^{-E/K_B T} \quad (3)$$

where T is temperature, while E and s are the trap depth and frequency factor, respectively. Note that the thermal stability of quartz OSL signal is known to follow the first order kinetics (e.g. Murray and Wintle 1999).

The theoretical trap filling ratio (n/N) can be approximated in practice by dividing the measured natural signal intensity (L_{nat}) by its intensity at dose saturation (L_{max}). The latter (L_{max}) can be obtained by fitting the dose response curve as a function of dose ($D = \dot{D}t$) with $K=0$ in Eq. 2,

$$L(D) = L_{\text{max}} \left(1 - e^{-D/D_0}\right). \quad (4)$$

E and s values can similarly be obtained by setting $\dot{D}=0$ in Eq. 2.

$$L(t) = L_0 e^{-(se^{-E/K_B T}) \cdot t} \quad (5)$$

where L_0 is the initial signal intensity, K_B is the Boltzmann's constant, and t is the storage time.

Using n/N , the apparent age (t_{app}) is,

$$t_{\text{app}} = -\frac{D_0}{\dot{D}} \ln \left(1 - \frac{n}{N}\right). \quad (6)$$

The apparent (mean storage) temperature (T_{app}) can be calculated, assuming $\frac{dn}{dt} = 0$ in Eq. 2,

$$\frac{\dot{D}}{D_0} \left(\frac{N}{n} - 1\right) = se^{-E/K_B T_{\text{app}}}. \quad (7)$$

When Eq. 7 is solved for T_{app} ,

$$T_{\text{app}} = -\frac{E}{K_B \ln \left[\frac{\dot{D}}{sD_0} \left(\frac{N}{n} - 1\right) \right]}. \quad (8)$$

3 Application of OSL thermochronology and thermometry for fault gouge

In this study, we assume an apparent OSL age of a fault gouge is a result of repetitive uniform partial resetting by large earthquakes and the natural signal intensity reached a steady state. A conceptual diagram of the steady state signal level after multiple partial resetting is shown in Fig. 1a. This assumption involves three parameters, (1) recurrence interval of earthquakes ($t_{\text{recurrence}}$), (2) shear heating temperature during an earthquake (T_{event}), and (3) the event duration (t_{event}) (Fig. 1b). To a good approximation (see below), the thermal loss coefficient $K(T_{\text{app}})$ at the apparent storage temperature, is proportional to a single-event $K(T_{\text{event}})$ through their respective timescales:

$$K(T_{\text{app}}) = \frac{t_{\text{event}}}{t_{\text{recurrence}} + t_{\text{event}}} K(T_{\text{event}}) \tag{9}$$

Note that the only assumption underlying Eq. 9 is that the loss of the OSL signal at the ambient environmental temperature in between any two heating events is negligible. This assumption should be valid by considering that the Partial Retention Zone (PRZ) of luminescence chronometers starts only above $\sim 30^\circ\text{C}$ (Guralnik et al. 2015; Guralnik and Sohbaty 2019). Finally, by combining Eqs. 3, 8 and 9, one obtains:

$$T_{\text{event}} = \frac{E}{K_B \left\{ -\ln \left[\frac{\dot{D}}{sD_0} \left(\frac{N}{n} - 1 \right) \right] + \ln \left(\frac{t_{\text{event}}}{t_{\text{recurrence}} + t_{\text{event}}} \right) \right\}} \tag{10}$$

which is the central new result of this study. Equation 10 allows to convert (semi-)measurable OSL quantities (n/N , \dot{D} , D_0 , E and s) into the shear heating temperature during an earthquake, given a known earthquake recurrence interval and the heating duration. For all practical reasons, the last fraction in the denominator

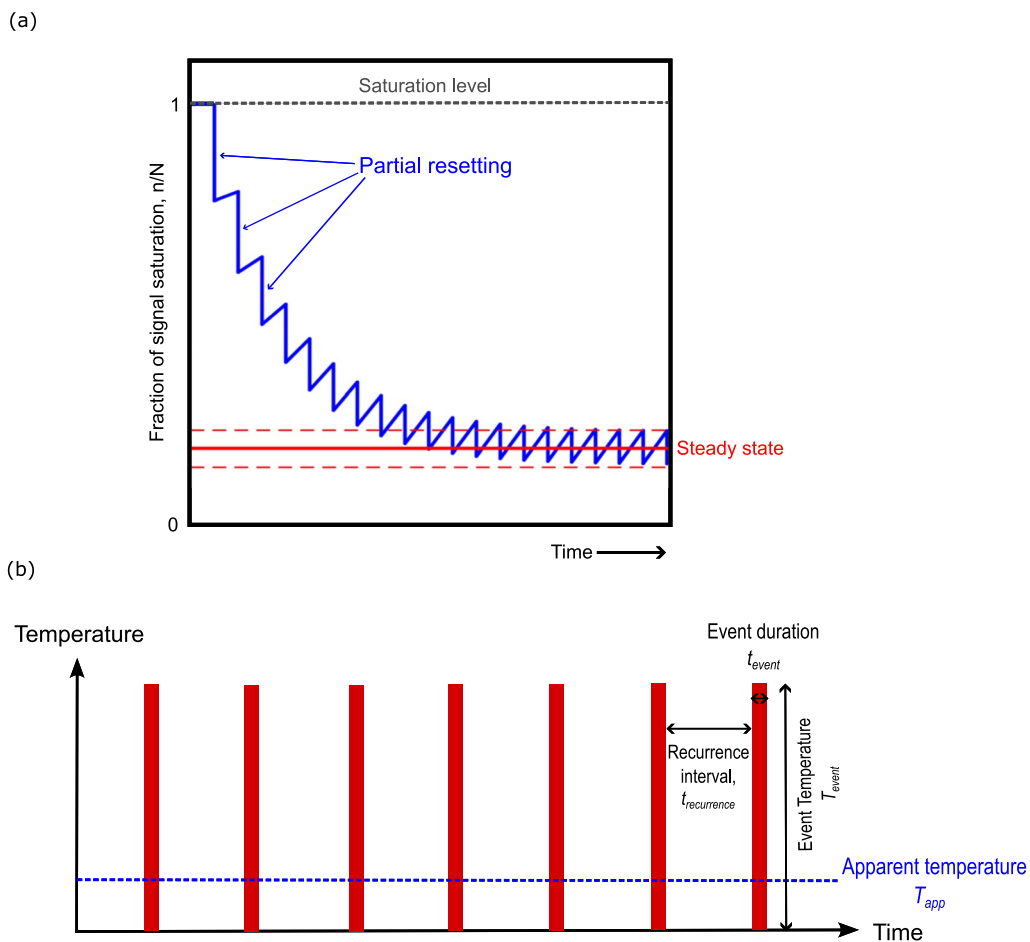


Fig. 1 Conceptual diagrams for **a** repetition of partial resetting by earthquakes, which bring the OSL signal to a steady-state level and **b** apparent temperature (T_{app})

of Eq. 10 can be approximated as $t_{\text{event}}/t_{\text{recurrence}}$, since a typical t_{event} would be on the order of seconds, while $t_{\text{recurrence}}$ on the order of 10^2 – 10^4 years. From Eq. 9, it is evident that “more active” faults, i.e. those experiencing more intense shear heating and/or shorter recurrence interval, should have a higher T_{app} . To de-couple T_{app} (Eq. 9) into a more specific activity metric (e.g. assuming comparable recurrence interval and shear heating durations to infer heating temperature, or any other combination of three parameters with one unknown), the use of Eq. 10 is recommended.

4 Study area and sampling

The Atotsugawa Fault is a dextral strike-slip fault, and one of the most active faults in central Japan (Fig. 2). This fault lies at the north-western edge of the Hida Range (northern Japanese Alps), and outcrops for about 70 km, striking ENE–WSW (e.g. Matsuda 1966). Several faults that run parallel to the Atotsugawa Fault compose the Atotsugawa Fault System. This fault system is situated within the Niigata-Kobe Tectonic Zone, where a large concentration of tectonic strain as well as many historical large earthquakes were observed (Sagiya et al. 2000). The Hietsu Earthquake, with an estimated magnitude of

7.0–7.1, suggests a last activity of the fault in AD1858. Past studies using trench excavations revealed that there have been four events on this fault in the last 11 ka (Research Group of Atotsugawa Fault et al. 1989; Takeuchi et al. 2003). According to this, a mean recurrence interval was calculated to be 2.3–2.7 ka. From surface displacements of fluvial terraces, a mean lateral slip rate of 2–5 m/ka was calculated, whereas the vertical slip rate was ~ 1 m/ka uplifting towards northwest (Takeuchi et al. 2003). The right-lateral slip motion was assumed to have continued for ca. 700 ka, derived from the total displacement of ~ 3 km of rivers that flow towards the north.

Fieldwork and sampling for OSL dating were conducted at an outcrop at Itani ($36^{\circ} 18' 43''$ N, $137^{\circ} 06' 06''$ E), in the western part of the Atotsugawa Fault (Fig. 2). The NE–SW trending outcrop (Fig. 3) has been described in detail by Niwa et al. (2008). The study of Ganzawa et al. (2013) using quartz OSL and TL dating was also conducted using a sample from the same outcrop. The fault core consists of gouge, breccia and cataclaste developed in the host rocks of the Funatsu Granite (Triassic to Early Jurassic) and gneiss from the Palaeozoic Hida Metamorphic Rocks (Niwa et al. 2008). During our fieldwork, no clear evidence of recent displacements such as deformation in overlying fluvial deposit was found at the outcrop. However, the fault at the outcrop was most likely ruptured during the AD1858 Hietsu Earthquake, because it is located in the area of the most representative fault zone along the topographic trace of the Atotsugawa Fault.

Four gouge and breccia samples for OSL dating (ITN-1, -2, -3, and -4; Fig. 3) were collected either by pushing stainless steel tubes into the cleaned outcrop surface or by taking large blocks. ITN-1 is a grey to brownish grey gouge, ~ 20 – 30 cm thick; ITN-2 is a ~ 20 cm thick, light-brown gouge, and ITN-3 is a ~ 20 cm thick, light-grey breccia. ITN-4 is a thin black gouge, ~ 10 cm thick, and was dated by Ganzawa et al. (2013), using OSL and TL

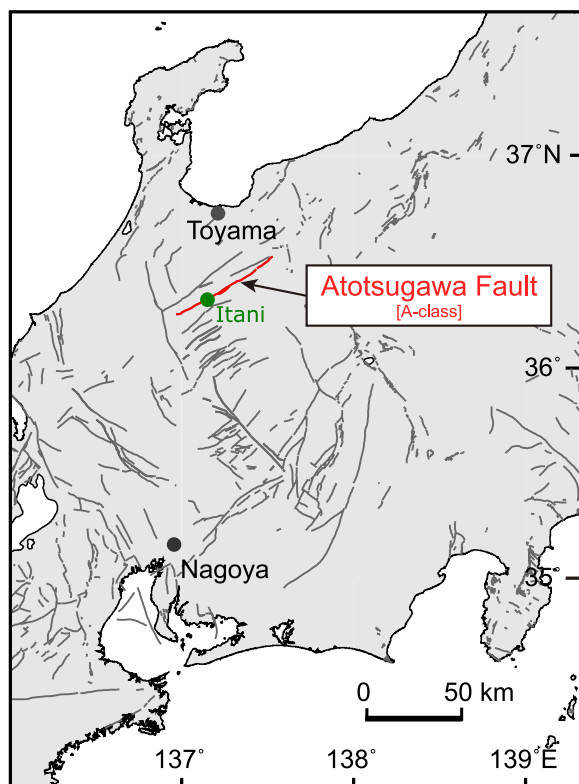


Fig. 2 Map of active faults in central Japan and the location of the Atotsugawa Fault

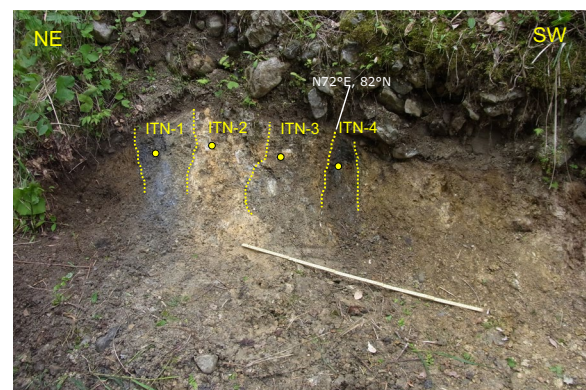


Fig. 3 Photo of the Itani outcrop and positions of OSL samples

with sand-sized grains. Between ITN-3 and -4 a shear plane of N72° E, 82° N was recognised (Niwa et al. 2008; Fig. 3). They also reported two K–Ar ages of illite close to the position of ITN-4, which ranged between 57 and 68 Ma; they interpreted that the temperature was never high enough (<100 °C; e.g. Pleuger et al. 2012) in the recent geological times to produce new clay minerals in the gouge. From the outcrop, no evidence of hydrothermal alteration can be seen, and thus possibility of past heating events other than earthquakes could be excluded.

5 Methods

5.1 Sample preparation

OSL sample preparations were conducted at the Luminescence Dating Laboratory at the Leibniz Institute for Applied Geophysics, Hannover, Germany, under subdued red-light conditions. After removing the materials that might have been exposed to light at both ends of the tubes and block surface, the light-protected inner part was treated with hydrochloric acid, sodium oxalate and hydrogen peroxide to remove carbonate, aggregates and organic matter, respectively. Fine-grained materials of either 4–11 µm (ITN-1, -3) or 1–11 µm (ITN-2, -4) were separated by repeated settling in water and centrifuge. The samples were then etched with hexafluorosilicic acid for 5 days to extract quartz. Aliquots for OSL measurements were prepared by settling 2 mg of sample material in distilled water onto aluminum discs.

The samples for dose rate measurements were freeze-dried at the Marine Science Department, Geological Survey of Japan. The dried samples were crushed and homogenised. The 50 g of material for each sample was sealed in a plastic container for gamma spectrometry measurements and stored at least 4 weeks to ensure the equilibrium of ^{222}Rn before measurement.

5.2 Dose rate measurements

High resolution gamma-ray spectrometry measurements were performed using an N-type Ortec pure Ge detector. The activity of U and Th series nuclides and ^{40}K obtained from the gamma measurements were converted to the concentrations of U, Th and K, and then calculated using the dose-rate conversion factors of Liritzis et al. (2013). The gamma-ray dose rates considering the effect of neighbouring layers were calculated following the method of Aitken (1985), using the R Luminescence package (Kreutzer et al. 2012). The natural water content and an α -value of 0.04 ± 0.02 (Rees-Jones 1995) were used to calculate dose rate.

5.3 OSL measurements

All OSL measurements were performed using two automated Risø TL/OSL DA-20 readers with blue and

infrared LEDs for optical stimulation and a $^{90}\text{Sr}/^{90}\text{Y}$ beta source for artificial irradiation. The quartz OSL signals revealed there was a strong contamination of a feldspar OSL signal, which was indicated by intense infrared stimulated luminescence (IRSL) signals. Therefore all OSL measurements were conducted using pulsed blue-light stimulation to remove feldspar OSL signals, with 50 µs on- and off-times (Denby et al. 2006; Ankjærgaard et al. 2010; Tsukamoto and Rades 2016). The pulsed OSL signal was detected only during the off-time, starting 5 µs after the LED pulses switched off to effectively remove the feldspar OSL signal. The natural signal intensity and the dose response curve of the OSL signal was measured with an post-IR OSL single-aliquot regenerative-dose (SAR) protocol pulsed blue stimulation for 200 s at 125 °C with a preheat of 180 °C for 10 s and a cut heat of 160 °C (Table 1). To further reduce the contribution of feldspar OSL in the blue OSL signal, a prior IR stimulation of 100 s at 125 °C was inserted before each pulsed OSL step. Since the on- and off-time ratio is 1:1, the actual light stimulation time for the pulsed OSL signal was 100 s. At least nine aliquots per each sample were measured to construct the dose response curve. Aliquots exceeding the recycling limit $\pm 15\%$ from unity were excluded from the calculation. The initial pulsed OSL signal for 1 s minus the immediate following signal for 4.5 s as the background was used for the pulsed OSL intensity calculation.

Using four aliquots each for all samples, a dose recovery test was conducted to check the validity of the applied SAR protocol. The aliquots were bleached using the blue LEDs in the reader twice for 300 s at room temperature and a beta dose of 180 Gy was given. This artificial dose was used as a surrogate natural dose and the measured against given dose ratio (dose recovery ratio) was calculated.

The thermal stability of the OSL signal was tested by an isothermal annealing test: one aliquot each of ITN-1, -2, -3, and -4, were irradiated with a beta dose of 200 Gy,

Table 1 Pulsed OSL SAR protocol

	Treatment	Observation
1	Dose	
2	Preheat 180 °C 10 s	
3	CW IRSL 125 °C 100 s	
4	Pulsed OSL 125 °C 200 s (50 µs on/off)	L_x
5	Test dose	
6	Cutheat 160 °C 0 s	
7	CW IRSL 125 °C 100 s	
8	Pulsed OSL 125 °C 200 s (50 µs on/off)	T_x
9	Back to 1	

then heated at 220, 240 and 260 °C for different holding times between 10 and 5120 s, and then the decrease of normalised OSL intensity was plotted against the isothermal holding time.

5.4 Apparent age and temperature

Using accepted aliquots of the dose response curve measurements, the mean n/N and D_0 values were calculated from Eq. 4. The thermal stability parameters, E and s were estimated by fitting the isothermal decay data using Eq. 5. Then the apparent age (t_{app}) and the apparent storage temperature (T_{app}) were derived from Eqs. 6 and 8, respectively.

5.5 Partial resetting condition

As we described above, we assume that the apparent OSL age of fault gouge was the result of multiple partial resettings by earthquakes with three parameters; (1) the recurrence interval of earthquakes ($t_{recurrence}$), (2) shear heating temperature at earthquakes (T_{event}), and (3) the event duration (t_{event}) (Fig. 1b, Eq. 9). In the case of the Atotsugawa Fault, only the recurrence interval is known to be ~ 2.5 ka. Therefore we solved Eq. 10 for T_{event} for a given t_{event} . Additionally, the sensitivity of T_{event} to the recurrence interval was investigated, by changing $t_{recurrence}$ one order of magnitude in either direction.

6 Results

Figure 4 shows continuous-wave (CW) and pulsed OSL signal of ITN-1 together with the prior IRSL signal after an irradiation of 200 Gy and a preheat of 180 °C for 10 s. The initial intensity of the pulsed post-IR OSL is only 24% of that of the CW OSL, indicating that the CW post-IR OSL signal is still dominated by the signal from contaminated feldspar, and the pulsed OSL simulation helped remove the contaminated feldspar OSL signal.

The dose rate is summarised in Table 2. The dose rate shows a large difference between the two neighbouring gouges of ITN-1 and -2, 1.31 ± 0.06 Gy/ka and 6.27 ± 0.49 Gy/ka, respectively, whereas those of ITN-3 and -4 are similar, ~ 2.6 Gy/ka. Figure 5 shows the OSL dose response curve of ITN-1. The fraction of signal saturation (n/N) is relatively uniform, from 0.30 ± 0.02 (ITN-2) to 0.39 ± 0.03 (ITN-3), i.e. considerably below the saturation. The dose recovery ratios are generally satisfactory, with the mean ratio of 0.98 ± 0.07 for all aliquots.

The apparent OSL ages between 22 ± 1 ka (ITN-2) and 72 ± 4 ka (ITN-1). When these ages are compared with the last large earthquake of the Atotsugawa Fault, which occurred in AD1858, the ages are two orders of magnitude older, indicating that the past earthquakes only partially reset the OSL signal.

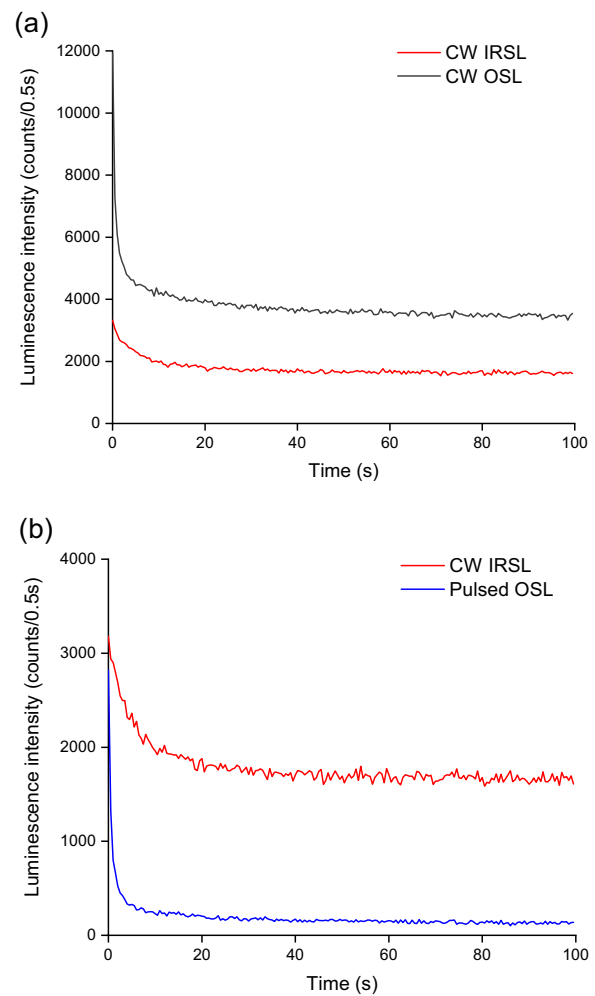


Fig. 4 **a** Continuous-wave and **b** pulsed OSL signals of quartz from ITN-1 and prior IRSL

The mean thermal stability parameters (E and s) are 1.64 ± 0.08 (eV) and $10^{13.13 \pm 0.77}$ (s^{-1}) (Fig. 6), which are consistent with the reported values of the quartz OSL fast component (e.g. Murray and Wintle 1999). Using all parameters, the apparent temperature, T_{app} was calculated, yielding 50 ± 6 °C (ITN-1) to 56 ± 6 °C (ITN-2), with a mean value of 53 ± 1.4 °C (Table 3). Table 3 shows n/N , D_0 , t_{app} and T_{app} for all samples. The t_{app} and T_{app} of all samples are plotted in Fig. 7.

Possible partial resetting conditions calculated for individual samples are shown in Fig. 8 using $t_{recurrence} = 2.5$ ka. Since all curves in Fig. 8 are close to each other, the calculation was also done using the mean parameters of the samples (Table 3) and $t_{recurrence} = 2.5$ ka, alongside two extreme end-members for comparison (0.25 ka and 25 ka; Fig. 9a). Any combination of t_{event} and T_{event} on each curve can explain

Table 2 Radioactivity and dose rate of the samples from Itani

Sample ID	K (%)	Th (ppm)	U (ppm)	Water (%)	Dose rate (Gy/ka)
ITN-1	0.62 ± 0.04	1.27 ± 0.06	1.37 ± 0.06	10	1.31 ± 0.06
ITN-2	3.78 ± 0.10	31.0 ± 0.30	1.77 ± 0.07	15	6.27 ± 0.49
ITN-3	1.55 ± 0.07	4.81 ± 0.13	1.55 ± 0.07	14	2.56 ± 0.17
ITN-4	1.65 ± 0.07	7.00 ± 0.15	2.23 ± 0.08	22	2.60 ± 0.13

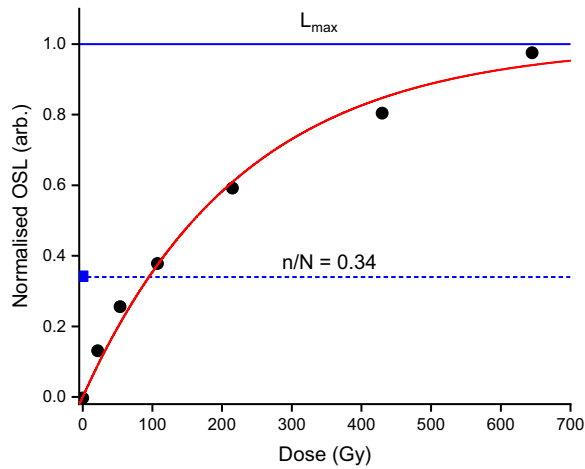


Fig. 5 Pulsed-OSL SAR dose response curve of for all accepted aliquots of ITN-1

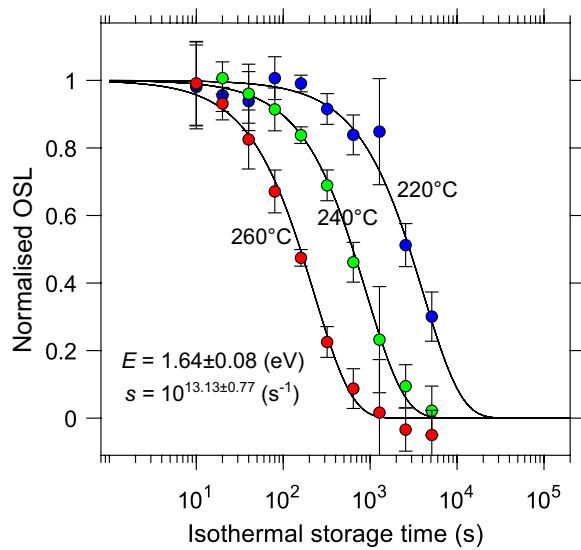


Fig. 6 Result of the isothermal annealing experiment of the pulsed OSL signal. The mean intensity of all four samples were plotted

Table 3 Fraction of signal saturation (n/N), characteristic saturation dose (D_0), apparent age (t_{app}), and apparent temperature (T_{app})

Sample ID	n/N	D_0 (Gy)	t_{app} (ka)	T_{app} (°C)
ITN-1	0.34 ± 0.02	229 ± 28	72 ± 4	50 ± 6
ITN-2	0.30 ± 0.02	389 ± 71	22 ± 1	56 ± 6
ITN-3	0.39 ± 0.03	259 ± 34	50 ± 4	52 ± 6
ITN-4	0.33 ± 0.04	233 ± 63	36 ± 2	53 ± 6
Mean	0.34 ± 0.02	278 ± 38	45 ± 11	53 ± 1

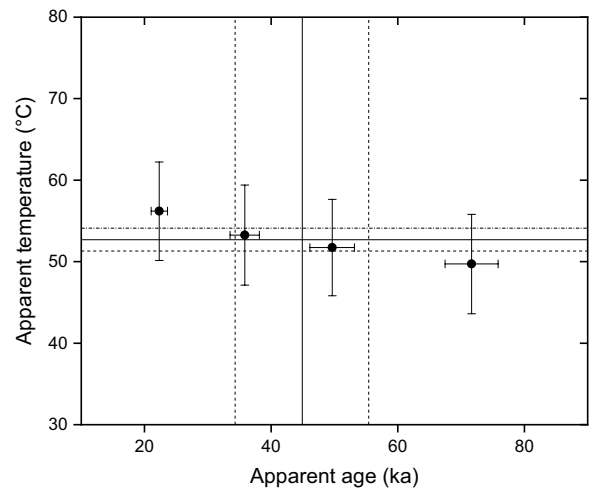


Fig. 7 Comparison of apparent age (t_{app}) and apparent temperature (T_{app}) for ITN-1, -2, -3 and -4

the mean apparent age of the samples. For the 2.5 ka recurrence, if the event duration is 1 s (e.g. Rice 2006),

the corresponding event temperature is ~300 °C, whereas for the duration of 10 s, the temperature drops to ~260 °C. In Fig. 9b, a comparison of three different event durations (0.1, 1 and 10 s) were made for different recurrence intervals. From these comparisons in Fig. 9, it is evident that T_{event} is insensitive to $t_{recurrence}$, as would be expected given that both time parameters ($t_{recurrent}$, t_{event}) appear within a logarithm in Eq. 10.

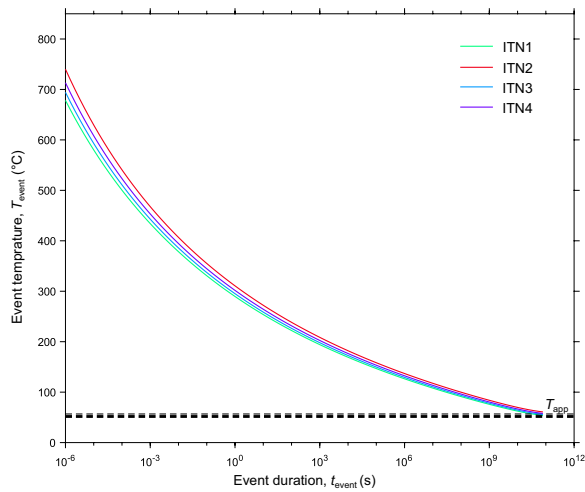


Fig. 8 Possible partial resetting conditions, calculated from n/N , D_0 , and \dot{D} for each sample

7 Discussion and conclusions

The OSL dating of fine-grained quartz extracted from the gouge and breccia samples of the Atotsugawa Fault yielded much older apparent ages (t_{app}), ranging between 22 ± 1 and 72 ± 4 ka, than the known most recent event of the fault in AD1858. The apparent ages are scattered, affected by the highly variable dose rate, which ranges from 1.31 ± 0.06 to 6.27 ± 0.49 Gy/ka. Whereas the t_{app}

is directly proportional to the dose rate (\dot{D}) (Eq. 6), both n/N and T_{app} have much less influence by the difference in dose rates, and yield similar values ranging between 0.30 ± 0.02 and 0.39 ± 0.03 , and between 50 ± 6 and 56 ± 6 °C, respectively. Similar results of a comparison between apparent ages and temperatures were reported by Guralnik et al. (2015) using the feldspar OSL signal from the German Continental Drilling Program (KTB) borehole (their Fig. S9 and Table S9).

Although apparent ages can still be used as maximum ages of the most recent event (e.g. Prince et al. 2024), when they are two orders of magnitude older, such information is meaningless. From the relatively uniform n/N and T_{app} of the four samples, we interpret that all the four gouges and breccias at the fault core experienced on average, similar thermal history, although the exact mechanism is not clear. We presume different earthquakes have occurred on different slip plains, but after many events, all the four samples have experienced similar thermal history, which resulted in the relatively uniform n/N . The natural OSL signal reached a steady-state level after multiple partial resetting events, or expressed as field saturation (Fig. 1a). This field saturation level translates to indefinite sample storage at $T_{app} = 53$ °C, which corresponds to T_{event} of ~ 300 °C for 1 s, at a recurrence interval of 2.5 ka. T_{app} can be used as metrics of fault activity, as these estimates are correlated with shear heating temperature

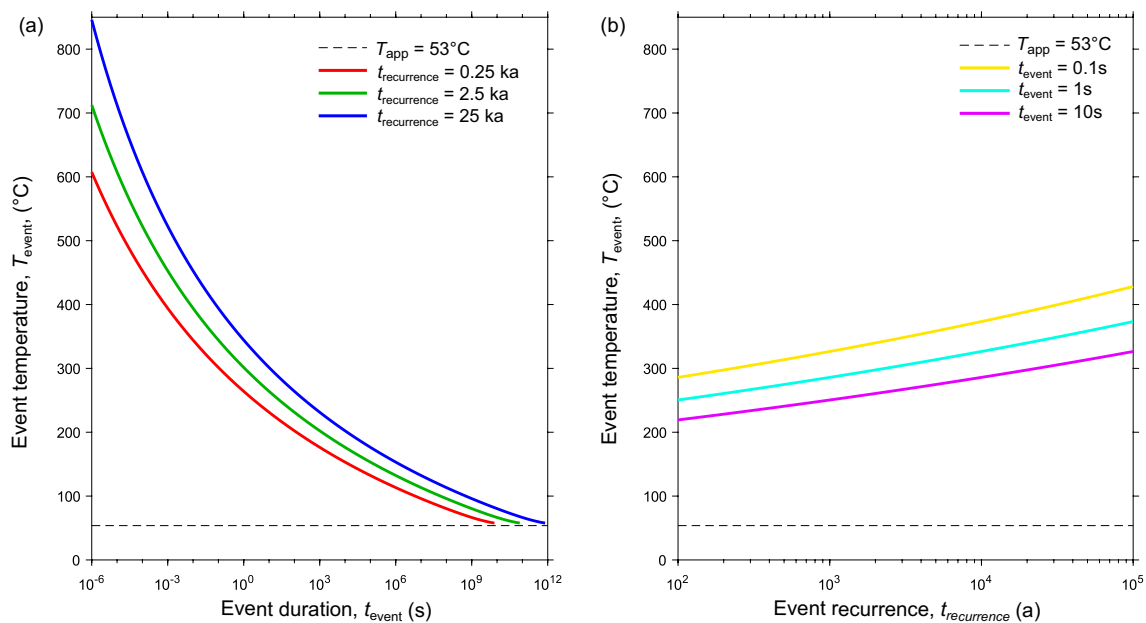


Fig. 9 **a** Nomogram for recurrent discrete heating event conditions of the Atotsugawa Fault using recurrence intervals of 0.25 ka, 2.5 ka, and 25 ka using the mean parameters of n/N , D_0 , and \dot{D} , and **b** that with event durations of 0.1, 1 and 10 s

(T_{event}) and/or duration (t_{event}), whilst anticorrelated with the recurrence interval, $t_{\text{recurrence}}$ (Eq. 10). Another potential advantage of our proposed method is that it could be widely applied to different luminescence and ESR signals with different saturation limits and thermal stabilities.

We calculated the possible temperature–time relationship for the past partial resetting condition of the Atotsugawa Fault, using the recurrence interval of 2.5 ka (Fig. 8 and 9a). The results calculated from the mean parameters suggest the event temperature of ~ 300 °C if the duration of shear heating is 1 s, and ~ 260 °C if the duration is 10 s. These conditions are similar to the observed time–temperature record of shear experiments with a slip rate of 1.3 m/s and a normal stress of 1 MPa (Kim et al. 2019; Oohashi et al. 2020).

In this work, we assumed a uniform recurrent partial resetting condition to explain the current OSL signal level, for the sake of simplicity (Fig. 1). However, the Atotsugawa Fault has a vertical slip component of ~ 1 m/ka, and thus it is possible that the gouge and breccia samples had gradually exhumed from shallow subsurface (up to ~ 170 m) within the dating range of the quartz OSL of ca. 170 ka, calculated from the mean 2 times D_0 (560 Gy) as the upper limit (Wintle and Murray 2006) divided by the mean dose rate of 3.2 Gy/ka (Tables 2 and 3). Whereas this depth does not reach the partial retention zone of the OSL signal, assuming a geothermal gradient of 26 °C/km measured from a borehole at Atotsugawa (Tanaka et al. 1999) and the mean ambient temperature of 11 °C, its overburden pressure was higher in the past (\sim up to a few MPa), which could be the reason of the high estimated the partial resetting temperature of ~ 300 °C. Oohashi et al. (2020) estimated the minimum depth for OSL partial resetting to be 37 m and 11 m for normal and reverse faults, respectively.

As a final note, if independent assumptions of shear-heating temperature and duration are available, via e.g. OSL sensitivity change (e.g. Rink et al. 1999), vitrinite reflectance geothermometry (e.g. Sakaguchi et al. 2011), and Raman spectroscopy of carboniferous materials (e.g. Beyssac et al. 2003), it would become possible to use Eq. 9 to infer a recurrence interval of presently undatable faults with currently unknown activity.

Acknowledgements

The authors are grateful to Masakazu Niwa, Toru Tamura, Kazumi Ito and students of Yamaguchi University for their supports and assistance for fieldwork. We thank Dave Tanner for discussion and language edits, and Saiko Sugisaki and technical staffs at AIST and LIAG for their assistance in the laboratory. Critical comments from two anonymous reviewers improved the clarity of the paper significantly.

Author contributions

Sumiko Tsukamoto: conception and design of the work; field and laboratory data acquisition; data analysis; interpretation of data; manuscript writing. Benny Guralnik: conception and design of the work; numerical modelling; interpretation of data; manuscript revisions. Erick Prince: numerical modelling; interpretation of data; manuscript revisions. Kiyokazu Oohashi: fieldwork planning; field data acquisition; interpretation of data; manuscript revisions. Makoto Otsubo: fieldwork planning; field data acquisition; interpretation of data.

Funding

Open Access funding enabled and organized by Projekt DEAL. This work was partially supported by a German Science Foundation project, no. 442590718.

Availability of data and materials

Data used for numerical modelling are available on request.

Declarations

Competing interests

There are no competing interests.

Author details

¹Leibniz Institute for Applied Geophysics, Stilleweg 2, 30655 Hannover, Germany. ²Department of Geosciences, University of Tübingen, Schnarrenbergstr. 94-96, 72076 Tübingen, Germany. ³Technical University of Denmark, 2800 Kgs. Lyngby, Denmark. ⁴Institute of Geological Sciences, Friedrich-Schiller University Jena, Burgweg 11, 07749 Jena, Germany. ⁵Graduate School of Sciences and Technology for Innovation, Yamaguchi University, Yamaguchi 753-8512, Japan. ⁶Geological Survey of Japan, AIST, Tsukuba Central 7, Higashi-1-1-1, Tsukuba, Ibaraki 305-8567, Japan.

Received: 4 August 2023 Accepted: 19 August 2024

Published online: 12 September 2024

References

- Aitken MJ (1985) Thermoluminescence dating. Academic Press, London
- Ankjærgaard C, Jain M, Thomsen KJ, Murray AS (2010) Optimising the separation of quartz and feldspar optically stimulated luminescence using pulsed excitation. *Radiat Meas* 45(7):778–785
- Beyssac O, Goffé B, Chopin C, Rouzaud JN (2003) Raman spectra of carbonaceous material in metasediments: a new geothermometer. *J Metamorph Geol* 20:859–871. <https://doi.org/10.1046/j.1525-1314.2002.00408.x>
- Chen YG, Chen YW, Chen WS, Lee KJ, Lee LS, Lu ST, Lee YH, Watanuki T, Lin YNN (2009) Optical dating of a sedimentary sequence in a trenching site on source fault of the 1999 Chi-Chi earthquake, Taiwan. *Quat Int* 199(1–2):25–33. <https://doi.org/10.1016/j.quaint.2009.01.001>
- Denby PM, Bøtter-Jensen L, Murray AS, Thomsen KJ, Moska P (2006) Application of pulsed OSL to the separation of the luminescence components from a mixed quartz/feldspar sample. *Radiat Meas* 41(7–8):774–779. <https://doi.org/10.1016/j.radmeas.2006.05.017>
- Durrani SA, Prachyabrued W, Christodoulides C, Fremlin JH, Edgington JA, Chen R, Blair IM (1972) Thermoluminescence of Apollo 12 samples: implications for lunar temperature and radiation histories. In: *Proceedings of the lunar science conference*, vol. 3, pp 2955–2970
- Durrani SA, Prachyabrued W, Hwang FSW, Edgington JA, Blair IM (1973) Thermoluminescence of some Apollo 14 and 16 fines and rock samples. In: *Proceedings of the lunar science conference*, vol. 4, pp 2465–2479
- Durrani SA, Khazal KAR, Ali A (1977) Temperature and duration of the shadow of a recently-arrived lunar boulder. *Nature* 266:411–415
- Fattahi M, Walker RT (2007) Luminescence dating of the last earthquake of the Sabzevar thrust fault, NE Iran. *Quat Geochronol* 2(1–4):284–289. <https://doi.org/10.1016/j.quageo.2006.06.006>
- Fukuchi T (1989) Increase of radiation sensitivity of ESR centres by faulting and criteria of fault dates. *Earth Planet Sci Lett* 94(1–2):109–122. [https://doi.org/10.1016/0012-821X\(89\)90087-3](https://doi.org/10.1016/0012-821X(89)90087-3)

- Ganzawa Y, Takahashi C, Miura K, Shimizu S (2013) Dating of active fault gouge using optical stimulated luminescence and thermoluminescence. *J Geol Soc Japan* 119(11):714–726. <https://doi.org/10.5575/geosoc.2013.0052>
- Guralnik B, Sohbati R (2019) Chapter 11: Fundamentals of Luminescence photo- and thermochronometry. *Advance in physics and applications of optically and thermally stimulated luminescence*. World Scientific, London, pp 399–437. https://doi.org/10.1142/9781786345790_0011
- Guralnik B, Jain M, Herman F, Paris RB, Harrison TM, Murray AS, Valla PG, Rhodes EJ (2013) Effective closure temperature in leaky and/or saturating thermochronometers. *Earth Planet Sci Lett* 384:209–218. <https://doi.org/10.1016/j.epsl.2013.10.003>
- Guralnik B, Jain M, Herman F, Ankjærgaard C, Murray AS, Valla PG, Preusser F, King GE, Chen RV, Lowick SE, Kook M, Rhodes EJ (2015) OSL-thermochronometry of feldspar from the KTB borehole, Germany. *Earth Planet Sci Lett* 423:232–243
- Herman F, Rhodes EJ, Braun J, Heiniger L (2010) Uniform erosion rates and relief amplitude during glacial cycles in the Southern Alps of New Zealand, as revealed from OSL-thermochronology. *Earth Planet Sci Lett* 297(1–2):183–189. <https://doi.org/10.1016/j.epsl.2010.06.019>
- Ikeya M, Miki T, Tanaka K (1982) Dating of a fault by electron spin resonance on intrafault materials. *Science* 215(4538):1392–1393. <https://doi.org/10.1126/science.215.4538.1392>
- Kim JH, Ree J-H, Choi J-H, Chauhan N, Hirose T, Kitamura M (2019) Experimental investigations on dating the last earthquake event using OSL signals of quartz from fault gouges. *Tectonophysics* 769:228191. <https://doi.org/10.1016/j.tecto.2019.228191>
- King GE, Herman F, Valla P, Guralnik B (2016) Trapped-charge thermochronometry and thermometry: a status review. *Chem Geol* 446:3–17. <https://doi.org/10.1016/j.chemgeo.2016.08.023>
- King GE, Tsukamoto S, Herman F, Biswas RH, Sueoka S, Tagami T (2020) Electron spin resonance (ESR) thermochronometry of the Hida range of the Japanese Alps: validation and future potential. *Geochronology* 2:1–15. <https://doi.org/10.5194/gchron-2-1-2020>
- Kreutzer S, Schmidt C, Fuchs MC, Dietze M, Fischer M, Fuchs M (2012) Introducing R package for luminescence dating analysis. *Anc TL* 30(1):1–8
- Lee HK, Schwarcz HP (1994) Criteria for complete zeroing of ESR signals during faulting of the San Gabriel fault zone, southern California. *Tectonophysics* 235(4):317–337. [https://doi.org/10.1016/0040-1951\(94\)90192-9](https://doi.org/10.1016/0040-1951(94)90192-9)
- Liritzis I, Stamoulis K, Papachristodoulou C, Ioannides K (2013) A re-evaluation of radiation dose-rate conversion factors. *Mediterr Archaeol Archaeom* 13(5):1–15
- Matsuda T (1966) Strike-slip faulting along the Atotsugawa Fault, Japan. *Bull Earthq Res Inst Univ Tokyo* 44:1179–1212. <https://doi.org/10.15083/0000033559>
- Murray AS, Wintle AG (1999) Isothermal decay of optically stimulated luminescence in quartz. *Radiat Meas* 30(1):119–125. [https://doi.org/10.1016/S1350-4487\(98\)00097-3](https://doi.org/10.1016/S1350-4487(98)00097-3)
- Niwa M, Shimada K, Kurosawa H, Miwa A (2008) Crush zone structure in a compressional step: an example of the western part of the Atotsugawa Fault. *J Geol Soc Japan* 114:495–515. <https://doi.org/10.5575/geosoc.114.495>
- Okumura K (2001) Paleoseismology in the Itoigawa-Shizuoka tectonic line in central Japan. *J Seismol* 5:411–431. <https://doi.org/10.1023/A:1011483811145>
- Oohashi K, Minomo Y, Akasegawa K, Hasebe N, Miura K (2020) Optically stimulated luminescence signal resetting of quartz gouge during subseismic to seismic frictional sliding: a case study using granite-derived quartz. *J Geophys Res Solid Earth* 125:e2020JB01990. <https://doi.org/10.1029/2020JB019900>
- Pleuger J, Mancktelow N, Zwingmann H, Manser M (2012) K-Ar dating of synkinematic clay gouges from Neopalpine faults of the Central, Western and Eastern Alps. *Tectonophysics* 550–553:1–16
- Prince EG, Tsukamoto S, Grützner C, Vrabec M, Ustaszewski K (2024) Not too old to rock: ESR and OSL dating methods reveal Quaternary activity of the Periadriatic Fault. *Earth Planets Space*. <https://doi.org/10.1186/s40623-024-02015-6>
- Rees-Jones J (1995) Optical dating of young sediments using fine-grain quartz. *Anc TL* 13(2):9–14
- Research Group for Active Faults of Japan (1991) *Active faults in Japan*. University of Tokyo Press, Tokyo
- Research Group for Atotsugawa Fault, Okada A, Takeuchi A, Tsukuda T, Ikeda Y, Watanabe M, Hirano S, Matsumoto S, Takehana Y, Okumura K, Kamishima T, Kobayashi T, Ando M (1989) A trenching study of the Atotsugawa fault at Nokubi, Miyagawa Village, Gifu Prefecture, central Japan. *J Geogr* 98(4):440–463. https://doi.org/10.5026/jgeography.98.4_440
- Rice JR (2006) Heating and weakening of faults during earthquake slip. *J Geophys Res Solid Earth* 111:B05311
- Rink WJ, Toyoda S, Rees-Jones J, Schwarcz HP (1999) Thermal activation of OSL as a geothermometer for quartz grain heating during fault movements. *Radiat Meas* 30:97–105. [https://doi.org/10.1016/S1350-4487\(98\)00095-X](https://doi.org/10.1016/S1350-4487(98)00095-X)
- Sagiya T, Miyazaki S, Tada T (2000) Continuous GPS array and present-day crustal deformation of Japan. *Pure Appl Geophys* 157:2303–2322. <https://doi.org/10.1007/PL00022507>
- Sakaguchi A, Chester F, Curewitz D, Fabbri O, Goldsby D, Kimura G, Li CF, Masaki Y, Screason EJ, Tsutsumi A, Ujiie K, Yamaguchi A (2011) Seismic slip propagation to the updip end of plate boundary subduction interface faults: vitrinite reflectance geothermometry on integrated ocean drilling program NanTro SEIZE cores. *Geology* 39(4):395–398. <https://doi.org/10.1130/G31642.1>
- Spencer J, Hadizadeh J, Gratier J-P, Doan M-L (2012) Dating deep? Luminescence studies of fault gouge from the San Andreas Fault zone 2.6 km beneath Earth's surface. *Quat Geochronol* 10:280–284
- Tagami T (2005) Zircon fission-track thermochronology and applications to fault studies. *Rev Mineral Geochem* 58:95–122
- Tagami T (2012) Thermochronological investigation on fault zones. *Tectonophysics* 538–540:67–85. <https://doi.org/10.1016/j.tecto.2012.01.032>
- Tagami T, Murakami M (2007) Probing fault zone heterogeneity on the Nojima fault: constraints from zircon fission-track analysis of borehole samples. *Tectonophysics* 443:139–152
- Takeuchi A, Ongirad H, Takebe A (2003) Recurrence interval of big earthquakes along the Atotsugawa fault system, central Japan: results of seismogeological survey. *Geophys Res Lett* 30(6):8011. <https://doi.org/10.1029/2002GL014957>
- Tanaka A, Yano Y, Sasada M, Okubo Y, Umeda K, Nakatsukasa N, Akita F (1999) Compilation of thermal gradient data in Japan on the basis of the temperatures in boreholes. *Bull Geol Surv Japan* 50(7):457–487
- Tsakalos E, Lin A, Kazantzaki M, Bassiakos Y, Nishiwaki T, Filippaki E (2020) Absolute dating of past seismic events using the OSL technique on fault gouge material—a case study of the Nojima Fault Zone, SW Japan. *J Geophys Res Solid Earth* 125:e2019JB01925. <https://doi.org/10.1029/2019jb019257>
- Tsukamoto S, Rades EF (2016) Performance of pulsed OSL stimulation for minimizing the feldspar signal contamination in quartz samples. *Radiat Meas* 84:26–33. <https://doi.org/10.1016/j.radmeas.2015.11.007>
- Tsukamoto S, Zwingmann H, Tagami T (2020) Chapter 7—Direct dating of fault movement. *Understanding faults*. Elsevier, Amsterdam, pp 257–282. <https://doi.org/10.1016/B978-0-12-815985-9.00007-2>
- Wintle AG, Murray AS (2006) A review of quartz optically stimulated luminescence characteristics and their relevance in single-aliquot regeneration dating protocols. *Radiat Meas* 41(4):369–391. <https://doi.org/10.1016/j.radmeas.2005.11.001>
- Zwingmann H, Yamada K, Tagami T (2010) Timing of brittle faulting within the Nojima fault zone, Japan. *Chem Geol* 275(3–4):176–185. <https://doi.org/10.1016/j.chemgeo.2010.05.006>

Publisher's Note

Springer Nature remains neutral with regard to jurisdictional claims in published maps and institutional affiliations.